CSIRO PUBLISHING

RESEARCH ARTICLE
https://doi.org/10.1071/MF25151

MARINE & FRESHWATER RESEARCH

Spatial variability in seawater chemistry across an intertidal mangrove–coral reef boundary

Alexander Waller[A,*], Kennedy Wolfe[A,B], Monique Webb[A], Thomas E. White[A], Lachlan Perris[C], Maria Byrne[A] and Shawna A. Foo[A]

For full list of author affiliations and declarations see end of paper

***Correspondence to:**
Alexander Waller
Marine Invertebrate Futures Group, School of Life and Environmental Sciences, The University of Sydney, Sydney, NSW 2006, Australia
Email: alexander.waller@sydney.edu.au

Handling Editor:
Martin Skov

Received: 7 July 2025
Accepted: 18 August 2026
Published: 30 September 2026

Cite this: Waller A *et al.* (2026) Spatial variability in seawater chemistry across an intertidal mangrove–coral reef boundary. *Marine and Freshwater Research* **77**, MF25151. doi:10.1071/MF25151

© 2026 The Author(s) (or their employer(s)). Published by CSIRO Publishing.
This is an open access article distributed under the Creative Commons Attribution-NonCommercial-NoDerivatives 4.0 International License (CC BY-NC-ND).

OPEN ACCESS

ABSTRACT

Context. Edge effects at habitat boundaries can generate strong physicochemical gradients that structure coastal ecosystems. Although environmental gradients within coexisting mangrove–coral habitats are well documented, spatial variability in seawater chemistry across intertidal mangrove–reef boundaries remains under-characterised. **Aim.** We examined fine-scale spatial variability in seawater chemistry across a mangrove–reef ecotone to assess how nearshore physicochemical conditions vary with proximity to mangroves. **Methods.** Seawater chemistry was measured over 2 weeks in Pioneer Bay, Orpheus Island (Great Barrier Reef, Australia), using sequential deployments of an autonomous sensor package and discrete daytime high- and low-tide sampling along a fine-scale mangrove-proximity gradient and beyond. **Key results.** Temperature, total-scale pH, salinity, PAR and wave power showed strong spatial structuring, whereas oxygen varied primarily with depth and time of day. Discrete sampling showed tide-dependent spatial patterns in temperature, total alkalinity and chlorophyll-*a* concentration, with the largest physicochemical shifts occurring at shallow nearshore sites closest to mangroves. **Conclusions.** Fine-scale physicochemical gradients occur across intertidal mangrove–reef boundaries without direct habitat coupling, modulated by depth and hydrodynamic exchange. **Implications.** The observed heterogeneity in seawater chemistry highlighted the need for seasonal, multi-site studies to resolve the extent and ecological significance of mangrove-associated processes on coral reef environments.

Keywords: carbonate chemistry, edge effects, environmental gradient, habitat boundaries, hydrodynamic exchange, intertidal, mangrove–coral reef ecotone, spatial variability.

Introduction

Edge effects, changes that occur at the boundary of two habitats (Clements 1907), have long been a focus of ecological research, particularly in terrestrial systems (e.g. forest boundaries), where fragmentation and human disturbance generate strong environmental gradients (Laurance and Yensen 1991; Ries and Sisk 2004). Along habitat edges, populations and communities may exhibit increased diversity (Murcia 1995; Harper *et al.* 2005), show little or no difference relative to habitat interiors (Connolly and Hindell 2006; Jankowski *et al.* 2021), or experience declines in species richness and diversity (Ewers and Didham 2006). In marine systems, edge effects have been widely explored in structured coastal habitats such as seagrass meadows (Tanner 2005; Connolly and Hindell 2006) and oyster reefs (Davenport *et al.* 2023), where responses range from enhanced diversity and productivity (Tanner 2005; Davenport *et al.* 2023), to neutral or negative effects driven by predation, physical disturbance, or altered environmental conditions (Tanner 2005; Connolly and Hindell 2006; Davenport *et al.* 2023). As in terrestrial ecosystems, edge effects in marine ecosystems are highly variable and influenced by habitat type, species interactions and local environmental conditions (Laurance and Yensen 1991; Ries and Sisk 2004). Ecological boundaries are therefore complex and multidimensional, with the magnitude and spatial position of a boundary differing by characteristics such as physical structure, light and physicochemistry (Cadenasso *et al.* 2003), particularly in coastal systems where multiple environmental gradients intersect.

Downloaded from connectsci.au/mf/article-pdf/doi/10.1071/MF25151/1972128/mf25151.pdf by guest on 25 November 2026

Mangrove habitats form a marine-terrestrial ecotone, establishing dynamic boundary systems shaped by strong interacting physical, chemical and biological gradients (Alongi 2008). Mangrove forests are diverse in form and setting, ranging from overwash and fringe systems to riverine and basin forests (Lugo and Snedaker 1974), which generate substantial spatial variation in depth, hydrodynamics, sedimentation and freshwater influence at mangrove–coastal boundaries (Krauss and Ball 2013). Consequently, environmental conditions experienced by marine communities near mangroves are highly context-dependent, governed primarily by geomorphology, depth and hydrodynamic exchange, rather than by the presence of mangroves alone or a single defining feature of mangrove habitats (Stewart *et al.* 2022). This highlights the uncertainty in both the strength and spatial extent of mangrove-associated physicochemical gradients across coastal systems.

In tropical regions, mangrove ecosystems form widespread and important coastal environments (Alongi 2002; Friess *et al.* 2019). Where mangroves occur in close spatial proximity to coral reefs, strong physical, chemical and biological gradients shape ecological structure and function (Camp *et al.* 2016; Carlson *et al.* 2021; Stewart *et al.* 2022; Waller *et al.* 2025). In these settings, depth and hydrodynamic exchange can modulate whether nearshore biogeochemical signals are amplified locally or diluted rapidly (Page *et al.* 2019; Cyronak *et al.* 2020), shaping the spatial footprint of edge effects across mangrove–coral reef boundaries (Stewart *et al.* 2022; Reithmaier *et al.* 2023). Boundaries between mangroves and adjacent reef habitats therefore provide insight into how environmental gradients at habitat interfaces influence marine communities (Camp *et al.* 2016; Stewart *et al.* 2022).

As observed in coexisting mangrove–coral (CMC) habitats, where corals live in direct association with mangroves, tightly coupled systems can strongly modify the environmental conditions experienced by corals (Camp *et al.* 2018; Stewart *et al.* 2022). In these systems, proximity to mangroves is associated with significant differences in seawater chemistry, oxygen availability, temperature, light attenuation and water flow (Stewart *et al.* 2022) because of the strong and highly variable environmental gradients characteristic of mangrove settings (Camp *et al.* 2018). Some CMC habitats may function as refugia for resident corals by reducing thermal and light stress under canopy-shaded conditions (Yates *et al.* 2014; Stewart *et al.* 2021), whereas others may precondition corals to future climate stressors by exposing them to extreme and highly variable physicochemical conditions (Camp *et al.* 2017, 2019; but see Scucchia *et al.* 2023).

In addition to CMC habitats, mangroves in tropical regions form extensive boundary habitats between terrestrial and coral reef ecosystems, often associated with reef flats or seagrass meadows that form an intermediate habitat (Carlson *et al.* 2021). Understanding how seawater chemistry varies across mangrove–coral reef boundaries is important to determine the spatial extent and structure of coastal physicochemical gradients (Saderne *et al.* 2019; Akhand *et al.* 2021; Pedersen *et al.* 2024). Research on coral–mangrove edge effects has primarily focused on environmental conditions within CMC habitats (Camp *et al.* 2018; Stewart *et al.* 2022). Alternatively, studies of mangrove-associated reef environments have largely examined habitat contrasts within mangrove–seagrass–coral mosaics, comparing mangrove forests, seagrass meadows and adjacent coral reefs at sites that are often separated by hundreds of metres to kilometres (e.g. Camp *et al.* 2016; Saderne *et al.* 2019; Akhand *et al.* 2021; de Jong *et al.* 2025). Thus, in these systems, environmental gradients span broad spatial scales and are associated with composite habitat transitions (Saderne *et al.* 2019; Akhand *et al.* 2021).

High benthic productivity and metabolism within seagrass and mangrove habitats can strongly modify local carbonate chemistry, generating physicochemical gradients across coastal seascapes that remain hydrodynamically connected to the open reef (Camp *et al.* 2016; Saderne *et al.* 2019; Akhand *et al.* 2021; Pedersen *et al.* 2024). However, the spatial gradients across open, intertidal mangrove–coral reef boundaries where mangroves and corals do not have a direct interface and seagrass is absent, remain poorly resolved. Thus, uncertainty persists over how far mangrove-associated signals in seawater chemistry extend into adjacent reef environments and how strongly they influence offshore coral habitats (Waller *et al.* 2025). Resolving spatiotemporal physicochemical variability across open mangrove–coral reef boundaries is critical for determining how rapidly conditions change with distance from shore and how co-occurring physical factors, such as depth and tidal exchange, influence coastal physicochemical variability and edge effects across mangrove–coral reef systems (Page *et al.* 2019; Cyronak *et al.* 2020).

This study aimed to characterise spatial variability in seawater chemistry along the boundary of a coastal mangrove–coral reef ecotone with an intervening reef flat at Orpheus Island, a continental island in the Great Barrier Reef (GBR), Australia. In contrast to other studies (e.g. Akhand *et al.* 2021; Pedersen *et al.* 2024; de Jong *et al.* 2025), seagrass habitat was not present. Using autonomous sensors for continuous seawater monitoring, alongside hand-held instruments for discrete water sampling, we examined how seawater chemistry varied with coral reef proximity to intertidal mangrove habitats. Typical of habitats at the land–sea interface (Wolfe *et al.* 2020; Carlson *et al.* 2021), we predicted that intertidal dynamics across the mangrove–coral reef ecotone would generate spatial gradients in seawater chemistry, with the magnitude and variability being determined by interacting effects of proximity to mangroves, distance from shore, depth and hydrodynamic exchange. This appears to be the first study focusing on a tidally flushed intertidal mangrove–coral reef boundary over a small (local) spatial scale, thereby extending our understanding of how fine-scale physicochemical gradients extend across coastal habitat boundaries under dynamic intertidal conditions.

Downloaded from connectsci.au/mf/article-pdf/doi/10.1071/MF25151/1972128/mf25151.pdf by guest on 25 November 2026

Materials and methods

Study sites

This study was conducted in Pioneer Bay (18°36′40″S, 146°29′11″E) on the leeward side of Orpheus Island, located on the inner shelf of the GBR, Australia (Fig. 1). Pioneer Bay spans ~1 km at its mouth, with an area of ~0.80 km^2 (George *et al.* 2019). The nearshore reef system of the bay features turbid conditions and a reef flat extending ~150 m from shore, characterised by patches of rubble and sand (O'Keeffe 1991; Hopley *et al.* 2007). Further seaward, the habitat transitions into a structurally complex reef crest, dominated by large colonies of *Porites* and *Acropora*, continuing into a deeper reef slope down to ~6-m water depth (Gordon *et al.* 2016; Oakley-Cogan *et al.* 2020). The southern shoreline is fringed by a 450-m stretch of mangrove forest (Fig. 1), primarily composed of *Rhizophora* spp., as well as *Bruguiera*, *Avicennia* and *Osbornia* spp. (George *et al.* 2019; S. Cannici, pers. comm.). These mangroves occur along the coast within an intertidal zone and are exposed at low tide and with an adjacent reef flat. No live corals occur sufficiently close to the mangrove shoreline to experience canopy shading at any point of the day. Several smaller, isolated mangrove patches are scattered along the northern beach, and episodic freshwater discharge enters the reef flat through the southern mangrove forest (Fig. 1) following periods of heavy rainfall, with the creek being typically stagnant under dry conditions.

To assess spatial variation in seawater chemistry across the mangrove–coral reef ecotone boundary, four sites were selected along the reef crest at increasing distances from the mangrove forest edge, spaced ~80 m apart and positioned to capture progressive changes in environmental conditions across the intertidal boundary gradient (Sites 1–4; Fig. 1). Site 1 was located 45 m from the shoreline and was the closest site to the mangroves, while ensuring established corals and sufficient water depth for deployment of autonomous sensors. In addition to the four gradient sites, we included one reef site at the opposite end of Pioneer Bay (Site 6) and a second reef site outside of the bay (Site 5; Fig. 1). Sites 5 and 6 were expected to have distinct hydrodynamic regimes with limited exposure to nearshore mangrove-associated conditions, providing spatial context beyond the immediate mangrove–coral reef ecotone. All sites were chosen ensuring continuous coral habitat and sufficient sensor deployment depth.

Seawater chemistry sampling regime

Seawater carbonate chemistry was characterised using a combination of continuous sensor-based measurements and

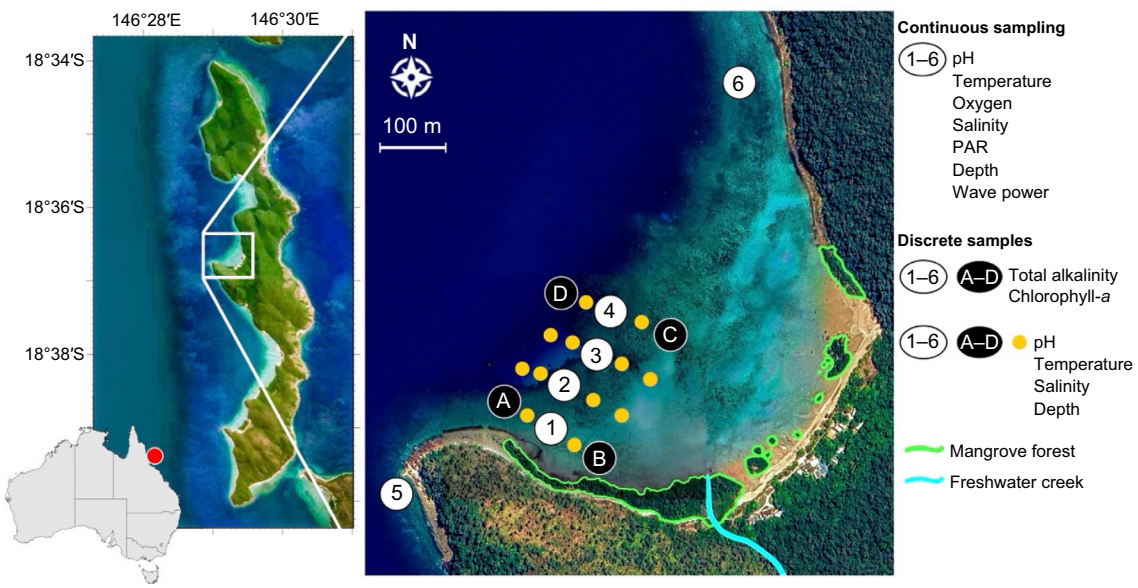


Fig. 1. Study location in Pioneer Bay, Orpheus Island (Great Barrier Reef, Australia), with aerial view of the mangrove forest, shallow water reef flat and coral reef habitats. We had six sites (white circles: Sites 1–6) where an autonomous sensor package was deployed for continuous seawater monitoring. Sites 1–4 represent an extending spatial gradient away from the mangrove forest, and Sites 5 and 6 represent reef sites beyond the immediate mangrove–coral reef ecotone boundary. Additional sites include black circles (A–D), where discrete seawater samples were collected for total alkalinity and chlorophyll-*a* analysis, and yellow dots, where point measurements of pH, salinity, temperature and depth were taken using a conductivity, temperature and depth (CTD) sensor and portable pH meter to assess tidal variability and increase spatial resolution across the mangrove–coral reef gradient. Figure has been created in *ArcGIS Pro* (ver. 3.4, see https://www.esri.com/en-us/arcgis/products/arcgis-pro/overview): 'World Imagery' Basemap (esri, Earthstar Geographics and the GIS User Community, see https://www.arcgis.com/home/item.html?id=10df2279f9684e4a9f6a7f08febac2a9, accessed 16 January 2024).

Downloaded from connectsci.au/mf/article-pdf/doi/10.1071/MF25151/1972128/mf25151.pdf by guest on 25 November 2026

discrete water samples. The study was conducted over 13 days in 2024 (1 July–13 July). Sampling was conducted over the Austral winter to provide a baseline characterisation of the influence of mangroves on local reef seawater chemistry without the impact of extreme summer light and temperature. Sites 1–6 were monitored during two separate 24-h intervals (~1 week apart), resulting in two 24-h deployment periods per site. Sites were sampled in a randomised order each week. Continuous sensor deployments were used to generate high-resolution data on seawater chemistry variability at each site; however, because sites were sampled sequentially rather than simultaneously, spatial comparisons among sites are interpreted as spatial patterns across the mangrove–coral reef ecotone, with potential influence from unmeasured diel variability.

Continuous seawater sampling

Continuous measurements were performed using a single sensor package comprising six autonomous instruments to monitor a suite of seawater chemistry parameters, including pH (total scale, pH_T), temperature, oxygen, salinity, photosynthetically active radiation (PAR), depth, wave power, wave energy and significant wave height (Hs). To ensure stability during sampling, sensors were secured to concrete blocks deployed at low tide, moved between sites every 24 h. Deployment and recovery times were recorded so that data collected during sensor transfers could be excluded, in addition to a sensor acclimation period of 45 min per site, the most conservative timeframe recommended by manufacturers (PyroScience, Aachen, Germany, see https://www.pyroscience.com/en/downloads, accessed 12 May 2024). Sensors remained submerged during transfers to prevent sensor caps from drying and interference from air exposure.

Oxygen, pH_T and temperature were measured using PyroScience AquapHOx-L-O2 and AquapHOx-L-pH loggers (10-min intervals). Sensors were calibrated before deployment, namely, the oxygen sensor with air-saturated water (100%) and deoxygenated water (0%), and the pH sensor with manufacturer-recommended National Institute of Standards and Technology (NIST) buffers (pH 2.0 and 11.0). Temperature was recorded on both sensors and cross-verified with the HOBO MX2022 Temperature and Light logger after deployment to ensure data accuracy and consistency (mean offset = −0.66 ± 0.03°C). Salinity and PAR were measured at 15-min intervals by using an Odyssey Conductivity and PAR Logger. The salinity logger was calibrated using factory calibration files, whereas the PAR logger was calibrated with a light source and a pre-calibrated integrating light meter (WALZ Diving-PAM Underwater Fluorometer). A linear calibration curve was generated from the logger and reference meter data, with the resulting slope and offset being applied to field data to adjust PAR to calibrated values.

Hydrodynamic parameters (depth, wave power, wave energy, Hs) were calculated using data from an RBRsolo3 tide and wave recorder (0.5-s intervals). Wave power and energy were derived from the wave spectrum analysis, calculated from surface elevation data using linear wave theory and a pressure response factor (Kp), as described by Karimpour and Chen (2017). Hs was computed using the zero-crossing method, which identifies points where the wave crosses the mean water level (Karimpour and Chen 2017). Wave energy was determined by integrating the wave spectrum by Fast Fourier Transform (FFT), with the zero-moment of the wave spectrum providing total wave energy (Karimpour and Chen 2017; Duce *et al.* 2022). Wave power, defined as the energy flux per unit wave crest length, was calculated by combining wave energy with group velocity (Karimpour and Chen 2017; Duce *et al.* 2022).

Discrete seawater sampling

Discrete sampling was designed to assess tidal variability and to increase spatial resolution within the sampling period. Total alkalinity (TA) and chlorophyll-*a* (Chl-*a*) concentration were measured from discrete water samples collected over a 3-day period (7–9 July 2024). Triplicate samples were collected from Sites 1–6 during daytime high and low tides (n = 3 per tide; six per site). Night samples were not collected because of logistical constraints. To construct a more robust spatial analysis of discrete measurements, TA and Chl-*a* concentration were also measured at Sites A–D (Fig. 1). At each site, 2 L of seawater was collected in a clean vessel and stored in a dark, cool container to prevent Chl-*a* degradation. Samples were returned to the laboratory where they were filtered immediately using 47-mm Whatman GF/F glass microfibre filters. The filtered volume was recorded with 300 mL per sample stored separately at 4°C for subsequent TA analysis, with this method of filtration and cold storage having been shown to be sufficient for TA stability as found in Mos *et al.* (2021).

After filtration, each filter paper was placed in a Falcon tube containing 10 mL of 90% acetone solution (9:1, acetone:distilled water), following protocols of chlorophyll-*a* determination in Dunton (2022), adapted from Jeffrey and Humphrey (1975). Filter papers were homogenised in the acetone solution, after which the Falcon tubes were wrapped in foil, and refrigerated for 16–24 h. Falcon tubes were then centrifuged at 500*g* for 15 min at 4°C, and the supernatant was analysed using a Vernier Go Direct SpectroVis Plus Spectrophotometer. Absorbance was measured at 750, 664, 647, 630 and 600 nm, and Chl-*a* concentrations (μg L^{-1}) calculated using a turbidity-corrected formula from Dunton (2022):

$$\text{Chl-}a = \frac{S[11.85(\text{Abs664}) - 1.54(\text{Abs647}) - 0.08(\text{Abs630})]}{V}$$

where S represents the volume of acetone used for extraction (mL), V is the volume of water filtered (L).

Downloaded from connectsci.au/mf/article-pdf/doi/10.1071/MF25151/1972128/mf25151.pdf by guest on 25 November 2026

Filtered seawater samples designated for TA analysis were transported in a cooler to the Sydney Institute of Marine Science and analysed within 1 month of collection. TA was determined by potentiometric titration using an 888 Titrando (Metrohm), following the method outlined by Harianto *et al.* (2021). The titration employed the Gran method to determine the second endpoint of the carbonate system, with accuracy and precision verified at ≤2 μmol kg^{-1} using certified reference materials (CRM Batch 123; Dickson *et al.* 2007).

To increase spatial resolution across the mangrove–coral reef ecotone and associated depth gradient, additional measurements of salinity, temperature and *in situ* pH (National Bureau of Standards scale) were collected in a grid pattern extending from the mangroves across the bay (yellow dots, Fig. 1). Measurements were taken using a SonTek CastAway CTD (factory calibrated) and an Orion Star A221 portable pH meter (calibrated daily using manufacturer-supplied Orion NIST-traceable buffer solutions; pH 4.01, 7.00, 10.01) during daytime high and low tides, concurrent with discrete sample collections. Portable pH measurements were recorded on the NBS scale (pH_{NBS}) and subsequently converted to the total hydrogen ion scale (pH_T) during carbonate system calculations using concurrent temperature, salinity and pressure data derived from Castaway CTD profiles in the *seacarb* package (ver. 3.3.3, see https://cran.r-project.org/package=seacarb) in *R* (ver. 4.5.1, R Foundation for Statistical Computing, Vienna, Austria, see https://www.r-project.org/). By contrast, the AquapHOx-L-pH sensor reported values directly on the total scale (pH_T). pH measurements were taken at a single point on the seafloor to capture bottom-water dynamics experienced at the level of the reef. As the CastAway instrument measured continuously across depth, salinity and temperature were calculated as averages across the entire water column, except at shallow sites during low tide, where a single point measurement was used. These measurements formed the basis of subsequent spatial analyses of seawater chemistry and associated carbonate system dynamics along the mangrove–coral reef gradient in Pioneer Bay.

Statistical analyses

To quantify spatial variation in seawater chemistry across the mangrove–coral reef ecotone in Pioneer Bay, linear mixed-effects (LME) models were applied to continuous 24-h sensor data collected at Sites 1–6 using a single sensor package deployed sequentially among sites. Analyses focused on the following two complementary spatial frameworks: (1) variation along the mangrove–coral reef gradient (Sites 1–4), and (2) comparisons between gradient sites and two reef sites beyond the gradient (Sites 5 and 6). All models were fitted using the full 24-h datasets, with inference centred on spatial patterns rather than diel contrasts or tide-matched comparisons.

For gradient analyses (Sites 1–4), distance from the mangrove forest was treated as a continuous fixed effect. Depth and time of day (day, night) were included as interacting fixed effects to account for diurnal and intertidal variation in seawater chemistry owing to the sequential sampling design. Time of day was classified on the basis of local sunrise (*c*. 06:45 hours) and sunset (*c*. 17:50 hours). Deployment period (Week 1, Week 2) was included as a random effect.

To compare mangrove–coral reef gradient sites with reef sites beyond this gradient, an additional LME was fitted, whereby site grouping (gradient sites *v*. Site 5 *v*. Site 6) was specified as a fixed effect. Depth and time of day were again included as interacting covariates, and deployment period as a random effect. *Post hoc* comparisons among site groups were conducted using estimated marginal means (EMM) part of the *emmeans* package (ver. 1.11.2, see https://CRAN.R-project.org/package=emmeans) in *R*. Collinearity was assessed using scatter plot matrices and variance inflation factors (VIF) (Zuur *et al.* 2010), leading to the exclusion of significant wave height (Hs) and wave energy because of their collinearity with wave power. Models were fitted using the lmer function in the *lme4* package (ver. 2.0.6, see https://CRAN.R-project.org/package=lme4; Bates *et al.* 2015) in *R*.

Carbonate system parameters, including dissolved inorganic carbon (DIC) and aragonite saturation state (Ω_{arag}), were calculated using temperature, salinity, TA and pH_T data in the *seacarb* package. Temperature and salinity were derived from Castaway CTD profiles, TA from an 888 Titrando (Metrohm), and pH_T was derived from converted Orion Star A221 measurements. Carbonate system calculations employed the dissociation constants of Mehrbach *et al.* (1973), refitted by Dickson and Millero (1987) for carbonic acid, and Dickson (1990) for boric acid. Orthophosphate and silicate concentrations were assumed negligible.

Discrete response variables (TA, DIC, pH_T, temperature, Chl-*a* concentration, and Ω_{arag}) were analysed using linear mixed-effects models (LMMs). As above, two complementary spatial frameworks were evaluated, including (1) a gradient-only model for Sites 1–4, where distance from the mangrove forest was treated as a continuous fixed effect, tidal state (high *v*. low tide) was included as a fixed effect, and their interaction was tested, and (2) a group model comparing gradient sites (Sites 1–4 pooled) against Sites 5 and 6, with tidal state included as a fixed effect and the interaction between tide and group tested. In both models, sampling date was included as a random intercept to account for repeated sampling across 3 consecutive days. *Post hoc* contrasts were conducted using EMM only where interaction terms were statistically significant, so as to resolve simple effects. For gradient models, this involved evaluating high *v*. low tide contrasts at site-specific distances and estimating linear distance slopes separately within each tidal state. For group models, this involved evaluating group contrasts within each tidal state. Where interaction terms were not significant, inference was based on main effects alone, without conducting site-specific or within-tide *post hoc* contrasts.

Downloaded from connectsci.au/mf/article-pdf/doi/10.1071/MF25151/1972128/mf25151.pdf by guest on 25 November 2026

To account for variations driven by salinity across sites, TA and DIC were normalised to a standard salinity of 35 (nTA and nDIC), assuming a zero freshwater TA/DIC end-member, consistent with previous reef carbonate chemistry studies (Suzuki and Kawahata 2003; Yates *et al.* 2014; Camp *et al.* 2016, 2017, 2019), reducing variability associated with freshwater input or evaporation, enabling more comparable carbonate system interpretations across sites (Friis *et al.* 2003; Courtney *et al.* 2021). Salinity-normalised nTA *v*. nDIC plots were used to assess dominant biogeochemical pathways influencing seawater chemistry across the mangrove–coral reef boundary. Standardised major axis (SMA; Type II) regression was applied to the relationship between nTA and nDIC by using mean values at high and low tides per site to account for uncertainty in both variables and characterise the overall covariance structure across sites (Suzuki and Kawahata 2003). A linear regression slope approaching a value of 2 indicates dominance of inorganic carbon cycling driven by calcification/dissolution (C/D) processes, whereas a slope near 0 suggests dominance of organic carbon cycling representing production/respiration (P/R) processes (Suzuki and Kawahata 2003; Kleypas *et al.* 2011).

Last, mean differences in discrete parameters (pH_T, temperature, salinity, TA, DIC, Ω_{arag}) between daytime high and low tides were calculated to conduct spatial analyses across Pioneer Bay. To characterise tidal fluxes in seawater chemistry experienced across the mangrove–coral reef gradient, spatial plots were developed using a radial basis function (RBF) spatial interpolation method in *ArcGIS Pro* (Buhmann 2000). Interpolation was restricted to gradient-aligned sites (Sites 1–4) and adjacent grid points (Sites A–D) to explore cross-shore and along-gradient spatial patterns in seawater chemistry. The RBF method was selected because of its ability to produce smooth, continuous surfaces, while ensuring that interpolated values pass exactly through measured points, making it well-suited for capturing gradual biogeochemical transitions across the mangrove–coral reef gradient (Li and Heap 2008; Arslan 2014). Compared with other interpolation methods, RBF effectively handles sparse datasets and minimises distortions, preserving the spatial structure of seawater chemistry parameters (Li and Heap 2008; Arslan 2014).

Results

Site characteristics

Water depth ranged from 0.23 to 3.75 m across low and high tides, with corals at Sites 1, B and C being occasionally exposed to air during extreme low tides. The mean depth of the continuously measured sites was relatively consistent (1.69–2.15 m), except at Site 1, which had a lower mean depth of 1.35 m. Depth was a significant predictor of all continuously measured seawater chemistry parameters throughout the diurnal cycle (Supplementary Table S1), highlighting its role in structuring environmental variability among sites. Mean water depth at sites where discrete water samples were collected (Sites 1–6, A–D) was 1.03 ± 0.09 m. During discrete sampling, Site C was the shallowest (0.60 ± 0.10 m), whereas Site D was deepest (2.82 ± 0.29 m).

Tidal patterns in Pioneer Bay varied throughout the study, characterised by mixed semidiurnal tides and an average tidal range of 1.46 ± 0.11 m across the two deployment weeks. A notable reduction in tidal range was observed in the second week (0.99 ± 0.16 m) compared with the first week (1.93 ± 0.06 m). Weather conditions also varied between deployment periods and were marked by partly cloudy skies with intermittent rainfall, particularly in Week 1 (28.0 mm) compared with Week 2 (17.8 mm). Average wind speed was 18.2 km h^{-1} (20.9 km h^{-1} in Week 1, 15.4 km h^{-1} in Week 2), predominantly from the south-east during all deployments.

Continuous seawater sampling

Spatial variation along the mangrove–coral reef gradient

Seawater chemistry varied along the mangrove–coral reef gradient (Sites 1–4), with distance from the mangrove forest significantly influencing temperature ($P = 0.04$), pH_T ($P < 0.001$), salinity ($P = 0.019$), PAR ($P = 0.01$) and wave power ($P < 0.001$) after accounting for depth, time of day and deployment period (Table S1, Fig. 2). Along the gradient, temperature and PAR increased with distance from the mangroves, whereas pH_T, salinity and wave power decreased (Supplementary Tables S1, S2). Oxygen concentrations were primarily structured by time of day and depth ($P < 0.001$) and did not vary with distance from the mangroves ($P = 0.061$; Table S1). Depth and time of day explained substantial variability across most parameters, with their interaction accounting for a significant portion of observed variability, apart from wave power, which showed no significant time of day effect or its interaction with depth ($P = 0.137$; Table S1).

Spatial contrasts between gradient and coral reef sites beyond the gradient

Seawater chemistry differed between mangrove–coral reef gradient sites (Sites 1–4) and reef sites beyond this gradient (Sites 5 and 6) after accounting for depth, time of day and deployment period (Fig. 2, Supplementary Table S3). Site grouping significantly influenced temperature ($P < 0.001$), salinity ($P < 0.001$), oxygen ($P < 0.001$), PAR ($P = 0.013$) and wave power ($P = 0.003$), whereas pH_T did not differ significantly among site groups ($P = 0.587$) among site groups (Table S3). Relative to the mangrove–coral reef gradient group, Site 5 exhibited significantly higher temperature, oxygen concentrations and PAR, but lower salinity and wave power values ($P < 0.05$; Tables S2, S4). Site 6 showed higher temperature but lower salinity than did the gradient

Downloaded from connectsci.au/mf/article-pdf/doi/10.1071/MF25151/1972128/mf25151.pdf by guest on 25 November 2026

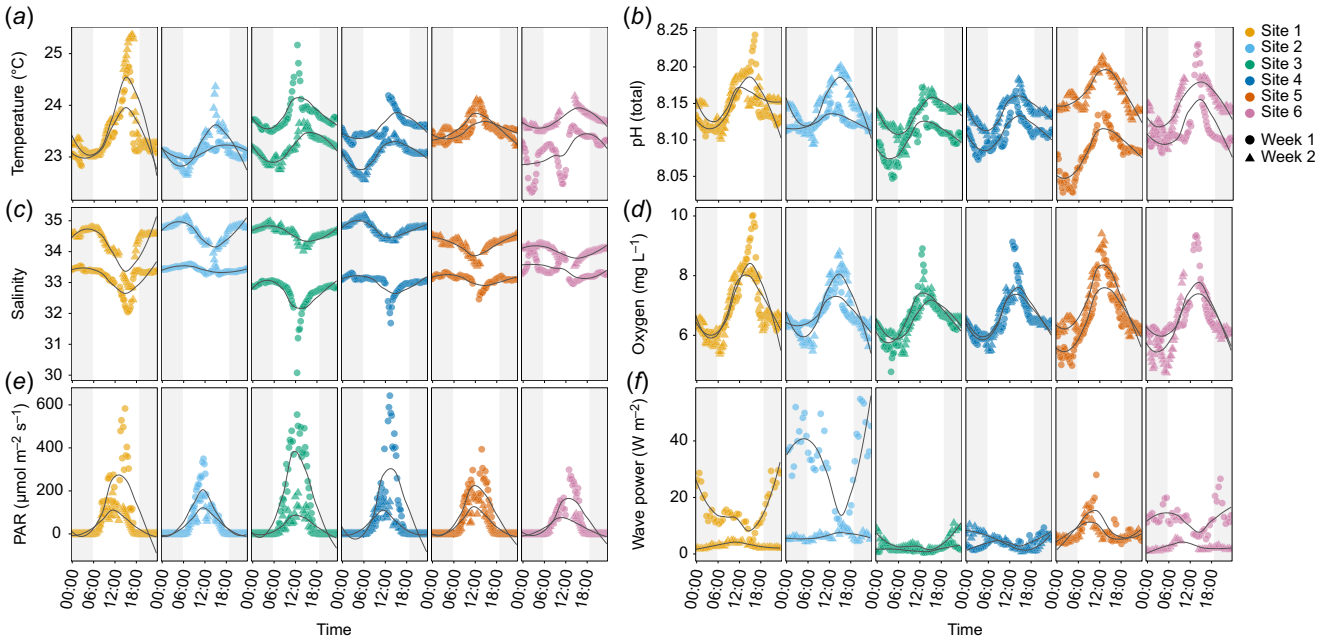


Fig. 2. Continuous sampling showing diel variation in seawater chemistry parameters across two deployment periods at Pioneer Bay, Orpheus Island, in 2024; (*a*) temperature, (*b*) pH_T, (*c*) salinity, (*d*) oxygen, (*e*) PAR, and (*f*) wave power. Night (grey) and day (white) intervals are defined on the basis of local sunrise and sunset during the sampling period. Sites, indicated by different-coloured symbols, are organised by proximity to mangrove forest, with Sites 5 and 6 representing reef sites beyond the mangrove–coral reef gradient. The black line represents a smooth trend line fitted across all data points to visualise general temporal structure, rather than site-specific diel co-occurrence.

sites, with no significant differences observed for oxygen, PAR, or wave power ($P \geq 0.139$; Supplementary Tables S2, S4). Between Sites 5 and 6, oxygen, PAR and temperature were higher at Site 5, whereas salinity was higher at Site 6 ($P \leq 0.031$, Tables S2, S4). pH_T and wave power did not differ significantly between Sites 5 and 6 ($P = 0.654$ and $P = 0.535$ respectively; Table S4).

Deployment-period variability

Temporal differences between deployment periods (Week 1 and Week 2) were significant across both analytical frameworks (Supplementary Tables S5, S6, S7, S8). Within the gradient-only analysis (Sites 1–4), deployment period significantly affected temperature, pH_T, salinity, PAR and wave power (all $P < 0.001$), whereas oxygen concentrations did not differ between weeks ($P = 0.09$; Table S5). During the second deployment period, temperature, PAR and wave power were lower, whereas pH_T and salinity were higher than in Week 1 (Table S6). Comparable deployment-period effects were observed when gradient sites were analysed with reef sites beyond the gradient (Sites 5 and 6), with significant effects detected for temperature, pH_T, salinity, PAR and wave power (all $P \leq 0.002$), but not for oxygen ($P = 0.277$) (Tables S7, S8).

Discrete seawater sampling

Spatial variation along the mangrove–coral reef gradient

Analysis of discrete seawater chemistry across the mangrove–coral reef gradient (Sites 1–4), showed parameter-specific tidal structure, with significant interactions between distance from the mangrove forest and tidal state (high, low) for temperature, TA and Chl-*a* concentration (Fig. 3, S1, Supplementary Table S9). Temperature varied with both tide and gradient position ($P < 0.001$; Table S9). At Sites 1–3, temperatures were significantly lower at high tide than at low tide (all $P \leq 0.002$; Supplementary Table S10), but this was not seen at Site 4 ($P = 0.546$; Table S10). Temperature also declined with an increasing distance from the mangrove forest at low tide ($P < 0.001$; Supplementary Table S11), but not at high tide ($P = 0.914$; Table S11, Fig. 3).

TA varied with the interaction between distance and tide ($P = 0.031$; Table S9). At the mangrove-proximal end of the gradient, TA was lower at high tide than at low tide at Sites 1 and 2 (for both, $P = 0.004$; Supplementary Tables S10, S12). No significant tidal difference was detected at sites further offshore (Sites 3 and 4, $P \geq 0.159$; Table S10). Consistent with this pattern, TA declined with an increasing distance from the mangrove forest at low tide ($P = 0.031$), but not at high tide ($P = 0.482$; Table S11).

Chlorophyll-*a* concentration also exhibited a significant interaction between distance and tide ($P < 0.001$; Table S9), declining with distance from the mangrove forest at high tide ($P < 0.001$) but not at low tide ($P = 0.496$; Table S11, Fig. S1). The influence of tide on Chl-*a* concentration varied among sites, with higher Chl-*a* concentration being measured at Site 1 at high tide ($P = 0.03$) and Site 4 at low tide ($P = 0.007$; Table S10). By contrast, there was no difference

Downloaded from connectsci.au/mf/article-pdf/doi/10.1071/MF25151/1972128/mf25151.pdf by guest on 25 November 2026

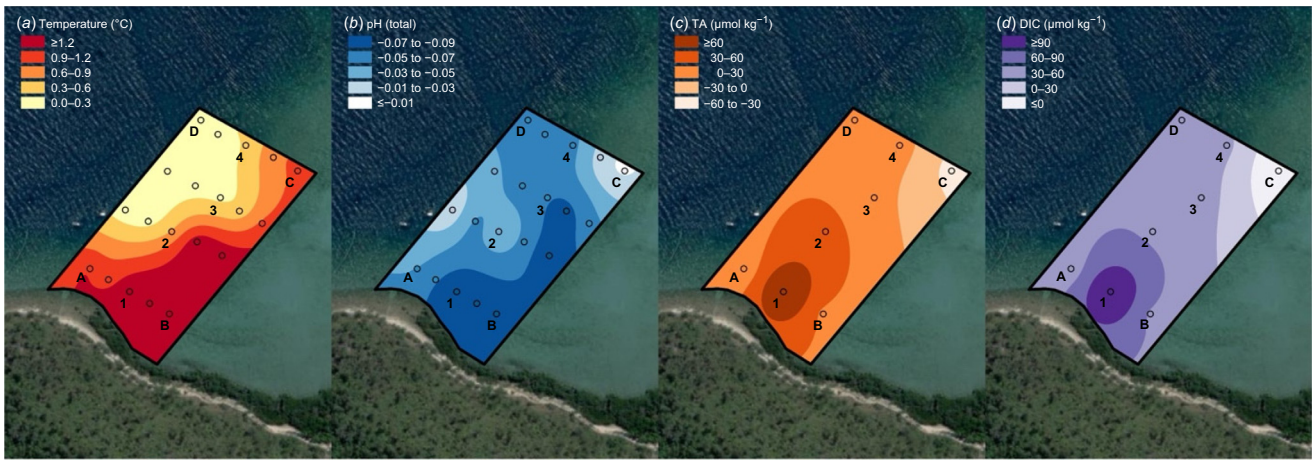


Fig. 3. Spatial plots using mean data collected from discrete water samples at Pioneer Bay, Orpheus Island, over 3 consecutive days (7–9 July 2024). Plots show differences between mean high and low tide in (*a*) temperature (°C), (*b*) pH_T, (*c*) total alkalinity (TA; µmol kg^{-1}), and (*d*) dissolved inorganic carbon (DIC; µmol kg^{-1}). Map source: esri, Maxar, Earthstar Geographics and the GIS User Community.

in pH_T, DIC and Ω_{arag} owing to the interaction of distance and tide ($P \geq 0.135$; Table S9). However, pH_T and DIC exhibited a significant main effect of tide ($P < 0.022$; Table S9), indicating that tidal variation was not expressed as a consistent spatial gradient.

Spatial contrasts between gradient and coral reef sites beyond the gradient

Discrete seawater chemistry showed limited spatial differentiation between mangrove–coral reef gradient sites (Sites 1–4 pooled) and reef sites beyond the gradient (Sites 5 and 6), with no significant main effect of site group or its interaction with tide detected for any parameter (all $P \geq 0.092$; Supplementary Table S13). However, tidal state influenced temperature ($P < 0.001$), pH_T ($P = 0.004$), DIC ($P = 0.013$) and Ω_{arag} ($P = 0.038$; Table S13). High- and low-tide contrasts were significant within the pooled gradient sites for temperature ($P < 0.001$), pH_T ($P = 0.034$) and DIC ($P = 0.015$; Supplementary Table S14). No site-specific tidal differences were detected at Sites 5 or 6 for any parameter (all $P \geq 0.129$; Table S14). No tidal effects were detected for TA or Chl-*a* concentration at any site (Table S13).

Relationship between TA and DIC

Regression analysis of salinity-normalised nTA *v.* nDIC showed a strong positive correlation (slope = 0.874, $R^2 = 0.804$; Fig. 4), on the basis of aggregated high- and low-tide means from discrete water samples. This indicates tightly coupled variation between nTA and nDIC across sites and tidal states, consistent with mixed contributions from organic (P/R) and inorganic (C/D; calcification/dissolution) metabolic pathways among sites. Across the mangrove–coral reef gradient (Sites 1–4) and adjacent sites (Sites A–D), nDIC and nTA were generally higher at low tide than at high tide, although both the magnitude and direction of tidal shifts varied spatially (Supplementary

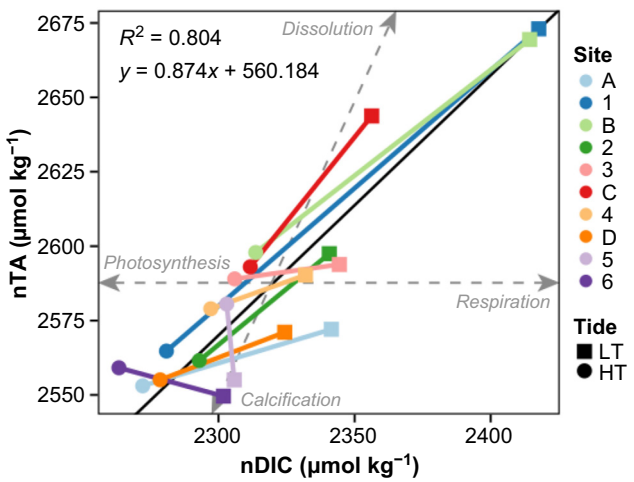


Fig. 4. Salinity-normalised (nTA *v.* nDIC) plots using aggregated values based on high-tide (HT, circles) and low-tide (LT, squares) points, with site-specific slopes reflecting tidal changes across sites, as indicated by different colour symbols. Data were collected from the discrete samples across six study sites (Site 1–6) and four additional Sites (A–D) at Pioneer Bay, Orpheus Island, over 3 consecutive days (7–9 July 2024). Grey dashed lines represent organic (production/respiration, P/R) and inorganic (calcification/dissolution, C/D) metabolic pathways. Solid black line shows the best fit line for all data points from a Type II major axis linear regression.

Table S15). Mangrove-proximal sites (Sites 1, 2, A and B) exhibited the largest positive tidal differences in both nDIC and nTA, with increases from high to low tide being consistent with shifts towards dissolution and respiration (Fig. 4, Supplementary Table S16). By contrast, sites located further from the mangrove forest generally showed smaller tidal changes in nDIC and nTA, whereas sites beyond the mangrove–coral reef gradient exhibited opposing tidal shifts (Fig. 4, Table S16). Site C exhibited the steepest positive slope among sites, indicating dominance of

Downloaded from connectsci.au/mf/article-pdf/doi/10.1071/MF25151/1972128/mf25151.pdf by guest on 25 November 2026

inorganic carbon cycling driven by C/D (Table S16). By contrast, Site 3 showed the weakest positive slope, suggesting dominance of organic carbon cycling owing to P/R (Table S16). Sites 5 and 6 exhibited negative slopes, with Site 5 exhibiting the largest inverse tidal shift, indicating inverse tidal shifts, relative to sites along the mangrove–coral reef gradient (Table S16). Overall, nTA–nDIC relationships varied spatially, with mangrove-proximal sites recording the largest tidal shifts in apparent metabolic balance across the mangrove–coral reef ecotone.

Discussion

This study characterised the spatial variability in seawater chemistry across the boundary of a direct, tidally flushed mangrove–coral reef ecotone across the reef flat in Pioneer Bay, Orpheus Island, where corals occur seaward of the mangrove canopy. Across the fine spatial scale investigated (<300 m) and mangrove-aligned gradient (Sites 1–4), several parameters showed consistent spatial structuring after accounting for depth, time of day and deployment period. This showed that measurable chemical and physical gradients can occur over fine spatial scales, even where a direct interface between mangrove and coral habitats is absent, and that coastal physicochemical variability can extend across intertidal reef flats into adjacent coral habitats at least at the spatial extent investigated here. This contrasts with mangrove–seagrass–coral reef mosaic studies, where environmental gradients are typically resolved across broader spatial scales (hundreds of metres to kilometres) and mediated by seagrass-dominated intermediate habitats (e.g. Saderne *et al.* 2019; Akhand *et al.* 2021).

Distance from the mangroves contributed to differences in temperature, pH_T, salinity, PAR and wave power, whereas oxygen was structured primarily by depth and time of day. The patterns observed here demonstrate how hydrodynamic exchange and depth can constrain the spatial footprint and expression of coastal biogeochemical signals at tidally flushed mangrove–coral reef boundaries with an intervening shallow reef flat. This reduces the accumulation of local chemical gradients as seen in mangrove–coral habitats with a direct interface and restricted water circulation, such as semi-enclosed lagoons and canopy systems (Camp *et al.* 2017, 2019; Maggioni *et al.* 2021; Stewart *et al.* 2022). As seen here, in open, tidally flushed systems, the hydrodynamic and physical context constrains the spatial reach of nearshore biogeochemical signals, resulting in steep attenuation of gradients across short distances. It is important to note that these spatial patterns detected here were documented during the austral winter, when thermal and light-driven forcing is weak. This shows that fine-scale heterogeneity in seawater chemistry can persist even under cooler seasonal conditions and may be amplified during warmer, more metabolically active periods.

Our continuous seawater sampling showed that depth was a dominant structuring factor in reef physicochemical variability, which is consistent with previous studies (Page *et al.* 2019; Cyronak *et al.* 2020). Across reef habitats, shallower waters generally exhibit greater variation in temperature and carbonate chemistry because benthic fluxes are expressed into a smaller volume of overlying water and are less diluted by mixing and exchange (Page *et al.* 2019; Cyronak *et al.* 2020). Although benthic communities can locally modify seawater chemistry through alterations to net community production and calcification (Page *et al.* 2016; Wolfe *et al.* 2018, 2021), depth and hydrodynamic context are likely to exert stronger control over seawater CO_2 system variability than is benthic community composition, particularly when considered across broader spatial scales (Takeshita *et al.* 2018; Page *et al.* 2019). In Pioneer Bay, the most nearshore site (Site 1) was shallower, on average, than were the other sites, and experienced intertidal exposure during extreme low tides, conditions expected to amplify physicochemical variability irrespective of mangrove proximity. Shallow environments are also more vulnerable to oxygen extremes and hypoxia under thermal stress, particularly where exchange is reduced and respiration dominates (Pezner *et al.* 2023). The spatial gradients observed along the ecotone boundary investigated here are most likely to reflect intersecting physical drivers (depth, exposure and circulation), on which any mangrove-associated influence is superimposed and potentially spatially constrained over short distances by reef flat processes.

Spatial patterns in total alkalinity (TA), dissolved inorganic carbon (DIC) and their salinity-normalised relationships provide insight into how biogeochemical processes operating at intertidal mangrove boundaries may be transmitted to adjacent coral reef habitats within tidally flushed mangrove–coral reef ecotones. Mangrove sediments are increasingly recognised as important sites of alkalinity production (Reithmaier *et al.* 2020, 2023), driven primarily by carbonate dissolution and anaerobic remineralisation (Saderne *et al.* 2021). These processes represent a substantial and previously overlooked component of coastal carbon cycling (Saderne *et al.* 2021; Reithmaier *et al.* 2023). Measurements across mangrove creeks and estuaries further demonstrate that mangroves can export both DIC and alkalinity to the coastal ocean (Sippo *et al.* 2016), with the relative balance of these fluxes determining whether mangroves act as local drivers or buffers of coastal acidification (Reithmaier *et al.* 2023). In Pioneer Bay, discrete measurements showed spatially structured tidal differences in nTA–nDIC relationships along the mangrove-aligned gradient, with shallower mangrove-proximal sites across the reef flat exhibiting the largest tidal shifts towards increased nTA and nDIC at low tide. We did not quantify lateral fluxes or directly attribute these patterns to mangrove export. However, the observed gradients are consistent with conceptual models in which mangrove sediments function as biogeochemical reactors (Saderne *et al.* 2021), whose chemical signatures may intermittently

Downloaded from connectsci.au/mf/article-pdf/doi/10.1071/MF25151/1972128/mf25151.pdf by guest on 25 November 2026

influence adjacent coastal waters (Sippo *et al.* 2016). This is modulated by tidal exchange, with short residence times constraining the persistence and spatial extent of these signals.

Spatial variation in salinity-normalised nTA–nDIC relationships further illustrate how carbonate system dynamics differ across the mangrove–coral reef ecotone in Pioneer Bay. The strong positive covariance between nTA and nDIC across sites and tidal states indicates that both organic carbon cycling (production/respiration) and inorganic carbon cycling (calcification/dissolution) contributed to observed variability, rather than did dominance by a single metabolic pathway. Despite the moderate overall slope, mangrove-proximal and shallow sites exhibited the largest increases in both nTA and nDIC at low tide, being consistent with a shift towards net respiration and carbonate dissolution in shallow and intertidal reef environments (Shaw *et al.* 2012; Cyronak and Eyre 2016). Similar responses have been documented in reef flats and intertidal systems, where low tide isolation enhances the influence of benthic metabolism on overlying seawater chemistry (Shaw *et al.* 2012; Wolfe *et al.* 2020), owing to multiple co-occurring processes operating across benthic communities, sediments and the water column (Takeshita *et al.* 2018; Page *et al.* 2019). However, in mangrove–seagrass–coral reef mosaics, carbonate system variability is influenced by strong metabolic modification within seagrass meadows and longer water residence times, which can amplify and spatially integrate biogeochemical signals across larger coastal domains (Saderne *et al.* 2019; Akhand *et al.* 2021; Pedersen *et al.* 2024). Overall, the spatial structure of nTA–nDIC relationships in the system investigated here indicated greater biogeochemical flux in shallower mangrove-proximal sites, as typical of intertidal and reef flat environments (Shaw *et al.* 2012; Cyronak and Eyre 2016; Page *et al.* 2019; Cyronak *et al.* 2020; Wolfe *et al.* 2020). Disentangling the relative contributions of intertidal boundary processes, benthic metabolism, hydrodynamic transport and mangrove-associated biogeochemical fluxes will require additional, targeted surveys. In particular, how far changes in these carbonate systems extend across reef flats to offshore coral habitats remains an unresolved question.

The two reef sites beyond the mangrove–coral reef gradient also differed from one another, providing insight into how physical setting shapes seawater chemistry independent of mangrove proximity. Site 6, located within Pioneer Bay but at the opposite end from the mangrove forest, closely resembled the gradient sites in continuously measured seawater chemistry, differing only in temperature and salinity, whereas Site 5, situated outside Pioneer Bay, differed across nearly all continuously measured parameters, consistent with greater exposure and mixing with the open ocean (de Jong *et al.* 2025). This suggests that Site 6, which shares the same semi-enclosed hydrodynamic setting as do the gradient sites, may better isolate mangrove-associated effects, whereas the stronger difference observed at Site 5 is likely to reflect distinct oceanographic exposure rather than reduced mangrove influence alone. Despite this, discrete carbonate chemistry parameters (TA, DIC, pHT and Ω_{arag}) did not differ significantly in mean values between the gradient sites and Sites 5 and 6. This indicates the presence of broadly comparable absolute carbonate conditions across the wider study area. However, the tidal covariance between nTA and nDIC differed significantly, with the gradient sites generally showing positive tidal shifts consistent with dissolution and respiration at low tide, whereas Sites 5 and 6 both showed inverse shifts, with Site 5 exhibiting the largest reversal, reflecting the distinct carbonate dynamics of offshore and reef-flat water masses relative to more terrestrially influenced nearshore waters (Suzuki and Kawahata 2003). This decoupling between comparable mean carbonate chemistry and contrasting tidal dynamics suggests that reef sites beyond the immediate gradient boundary may not be chemically distinct in terms of mean carbonate conditions but are instead governed by tidal-scale processes. This may reflect a reduced contribution of mangrove-derived respiration and dissolution signals relative to photosynthetic or hydrodynamically driven processes operating on a different tidal phase at more exposed reef locations (Takeshita *et al.* 2018; Page *et al.* 2019).

Variable rainfall represents an important source of background variability in coastal seawater chemistry and is a potential confounding factor here when interpreting spatial patterns derived from sequential sensor deployments, particularly in nearshore reef environments influenced by episodic freshwater input (Devlin *et al.* 2012; Fabricius *et al.* 2025). During the study period, intermittent rainfall occurred between deployment periods and was associated with measurable changes in salinity across Pioneer Bay, indicating episodic freshwater influence on the system. Freshwater inputs can alter seawater carbonate chemistry directly through dilution (Devlin *et al.* 2012), and indirectly by the delivery of terrestrially derived organic matter and nutrients (Volta *et al.* 2020), which can stimulate respiration and modify metabolic balance in adjacent reef waters. Such rainfall-driven inputs are well documented in coastal reef environments (Devlin *et al.* 2012) and estuarine systems (Volta *et al.* 2020), where circulation, residence time and geomorphology generate short-lived but spatially heterogeneous biogeochemical responses. In this study, deployment period was explicitly accounted for in all models to accommodate temporal variability associated with both climatic conditions and the rotating sensor design. Although it is likely that rainfall contributed to differences observed between deployment periods, spatial gradients along the mangrove–coral ecotone remained evident after accounting for deployment period, depth and time of day. This indicates that rainfall alone does not explain the observed spatial structuring. Moreover, freshwater influence in Pioneer Bay was episodic, with the largest salinity variability being detected in the central bay (Site 3, 30.08–34.98; Table S2) rather than consistently at shallower mangrove-proximal sites. This suggests that

Downloaded from connectsci.au/mf/article-pdf/doi/10.1071/MF25151/1972128/mf25151.pdf by guest on 25 November 2026

rainfall-related effects interact with local circulation and bathymetry rather than uniformly tracking depth and mangrove proximity.

Importantly, this study was conducted during the austral winter, when rainfall intensity, terrestrial runoff and biological activity are comparatively reduced relative to summer conditions on the Great Barrier Reef (Fabricius *et al*. 2025). The detection of coherent spatial patterns under these conservative seasonal conditions suggests that rainfall-modulated variability does not obscure underlying spatial structure across the mangrove–coral reef ecotone, but instead contributes to the broader environmental mosaic shaping nearshore reef chemistry. Together, these results highlight that the processes shaping seawater chemistry across direct, tidally flushed mangrove–coral reef ecotones lacking seagrass can differ from both CMC habitats and mangrove–seagrass–coral reef mosaics, where canopy cover, sediment retention, seagrass metabolism and restricted circulation exert stronger local control (Camp *et al*. 2017, 2018; Stewart *et al*. 2022).

This study has demonstrated that measurable and ecologically meaningful spatial variability in seawater chemistry can arise across direct, intertidal mangrove–coral reef boundaries with intervening reef flat habitats, even in the absence of direct habitat coupling between mangroves and corals. Across Pioneer Bay, spatial patterns in carbonate chemistry were structured primarily by physical context, with depth, exposure and hydrodynamic exchange constraining the magnitude of locally generated biogeochemical signals. The detection of significant gradients during the austral winter underscores that fine-scale heterogeneity in seawater chemistry can persist under conservative seasonal conditions. These patterns may intensify during warmer, more metabolically active periods. Indeed, nearshore physicochemical structure is strongly modulated by geomorphology and circulation, such that proximity to mangroves alone is insufficient to predict seawater chemistry as shown here. Intertidal position, depth and hydrodynamic exchange play a central role in shaping edge effects across mangrove–coral reef boundaries. Resolving how these physical drivers regulate cross-boundary biogeochemical exchange and constrain the spatial extent of coastal influence is therefore critical. This understanding will improve predictions of when and where mangrove-associated processes meaningfully influence coral reef communities, while helping to determine whether mangroves buffer or amplify climate-related stress across different coastal extents. Future studies combining simultaneous multi-site deployments across seasons, alongside direct measurements of water exchange and associated chemical transport across mangrove–coral reef boundaries, will be essential for quantifying the spatial reach of coastal influence across mangrove–coral reef systems under ongoing environmental change.

Supplementary material

Supplementary material can be accessed from the article page online.

References

Akhand A, Watanabe K, Chanda A, Tokoro T, Chakraborty K, Moki H, Tanaya T, Ghosh J, Kuwae T (2021) Lateral carbon fluxes and CO_2 evasion from a subtropical mangrove–seagrass–coral continuum. *Science of The Total Environment* **752**, 142190. doi:10.1016/j.scitotenv.2020.142190

Alongi DM (2002) Present state and future of the world's mangrove forests. *Environmental Conservation* **29**(3), 331–349. doi:10.1017/S0376892902000231

Alongi DM (2008) Mangrove forests: resilience, protection from tsunamis, and responses to global climate change. *Estuarine, Coastal and Shelf Science* **76**(1), 1–13. doi:10.1016/j.ecss.2007.08.024

Arslan H (2014) Estimation of spatial distribution of groundwater level and risky areas of seawater intrusion on the coastal region in Çarşamba Plain, Turkey, using different interpolation methods. *Environmental Monitoring and Assessment* **186**, 5123–5134. doi:10.1007/s10661-014-3764-z

Bates D, Mächler M, Bolker B, Walker S (2015) Fitting linear mixed-effects models using lme4. *Journal of Statistical Software* **67**(1), 1–48. doi:10.18637/jss.v067.i01

Buhmann MD (2000) Radial basis functions. *Acta Numerica* **9**, 1–38. doi:10.1017/S0962492900000015

Cadenasso ML, Pickett STA, Weathers KC, Jones CG (2003) A framework for a theory of ecological boundaries. *BioScience* **53**(8), 750–758. doi:10.1641/0006-3568(2003)053[0750:AFFATO]2.0.CO;2

Camp EF, Suggett DJ, Gendron G, Jompa J, Manfrino C, Smith DJ (2016) Mangrove and seagrass beds provide different biogeochemical services for corals threatened by climate change. *Frontiers in Marine Science* **3**, 52. doi:10.3389/fmars.2016.00052

Camp EF, Nitschke MR, Rodolfo-Metalpa R, Houlbrèque F, Gardner SG, Smith DJ, Zampighi M, Suggett DJ (2017) Reef-building corals thrive within hot-acidified and deoxygenated waters. *Scientific Reports* **7**, 2434. doi:10.1038/s41598-017-02383-y

Camp EF, Schoepf V, Mumby PJ, Hardtke LA, Rodolfo-Metalpa R, Smith DJ, Suggett DJ (2018) The future of coral reefs subject to rapid climate change: lessons from natural extreme environments. *Frontiers in Marine Science* **5**, 4. doi:10.3389/fmars.2018.00004

Camp EF, Edmondson J, Doheny A, Rumney J, Grima AJ, Huete A, Suggett DJ (2019) Mangrove lagoons of the Great Barrier Reef support coral populations persisting under extreme environmental conditions. *Marine Ecology Progress Series* **625**, 1–14. doi:10.3354/meps13073

Carlson RR, Evans LJ, Foo SA, Grady BW, Li J, Seeley M, Xu Y, Asner GP (2021) Synergistic benefits of conserving land–sea ecosystems. *Global Ecology and Conservation* **28**, e01684. doi:10.1016/j.gecco.2021.e01684

Clements FE (1907) 'Plant physiology and ecology.' (H. Holt: New York, NY, USA) doi:10.5962/bhl.title.28570

Connolly RM, Hindell JS (2006) Review of nekton patterns and ecological processes in seagrass landscapes. *Estuarine, Coastal and Shelf Science* **68**(3–4), 433–444. doi:10.1016/j.ecss.2006.01.023

Courtney TA, Cyronak T, Griffin AJ, Andersson AJ (2021) Implications of salinity normalization of seawater total alkalinity in coral reef metabolism studies. *PLoS ONE* **16**(12), e0261210. doi:10.1371/journal.pone.0261210

Cyronak T, Eyre BD (2016) The synergistic effects of ocean acidification and organic metabolism on calcium carbonate ($CaCO_3$) dissolution in coral reef sediments. *Marine Chemistry* **183**, 1–12. doi:10.1016/j.marchem.2016.05.001

Cyronak T, Takeshita Y, Courtney TA, DeCarlo EH, Eyre BD, Kline DI, Martz T, Page H, Price NN, Smith J, Stoltenberg L, Tresguerres M, Andersson AJ (2020) Diel temperature and pH variability scale with depth across diverse coral reef habitats. *Limnology and Oceanography Letters* **5**(2), 193–203. doi:10.1002/lol2.10129

Davenport TM, Grabowski JH, Hughes AR (2023) Edge effects influence the composition and density of reef residents on subtidal restored oyster reefs. *Restoration Ecology* **31**(1), e13693. doi:10.1111/rec.13693

Downloaded from connectsci.au/mf/article-pdf/doi/10.1071/MF25151/1972128/mf25151.pdf by guest on 25 November 2026

de Jong C, van Os I, Sepúlveda-Rodríguez G, de Baat ML, Schoepf V (2025) High-resolution temporal assessment of physicochemical variability and water quality in tropical semi-enclosed bays and coral reefs. *Science of The Total Environment* **968**, 178810. doi:10.1016/j.scitotenv.2025.178810

Devlin MJ, McKinna LW, Álvarez-Romero JG, Petus C, Abott B, Harkness P, Brodie J (2012) Mapping the pollutants in surface riverine flood plume waters in the Great Barrier Reef, Australia. *Marine Pollution Bulletin* **65**(4–9), 224–235. doi:10.1016/j.marpolbul.2012.03.001

Dickson AG (1990) Thermodynamics of the dissociation of boric acid in synthetic seawater from 273.15 to 318.15 K. *Deep-Sea Research – A. Oceanographic Research Papers* **37**(5), 755–766. doi:10.1016/0198-0149(90)90004-F

Dickson AG, Millero FJ (1987) A comparison of the equilibrium constants for the dissociation of carbonic acid in seawater media. *Deep-Sea Research – A. Oceanographic Research Papers* **34**(10), 1733–1743. doi:10.1016/0198-0149(87)90021-5

Dickson AG, Sabine CL, Christian JR (2007) 'Guide to best practices for ocean CO_2 measurements.' (North Pacific Marine Science Organization: Sidney, BC, Canada)

Duce S, Vila-Concejo A, McCarroll RJ, Yiu B, Perris LA, Webster JM (2022) Field measurements show rough fore reefs with spurs and grooves can dissipate more wave energy than the reef crest. *Geomorphology* **413**, 108365. doi:10.1016/j.geomorph.2022.108365

Dunton K (2022) Water column chlorophyll extraction. (UT Marine Science Institute: Port Aransas, TX, USA) Available at https://tpwd.texas.gov/landwater/water/habitats/seagrass/media/qapp/Chlorophyl_a_protocol.pdf

Ewers RM, Didham RK (2006) Confounding factors in the detection of species responses to habitat fragmentation. *Biological Reviews* **81**(1), 117–142. doi:10.1017/S1464793105006949

Fabricius KE, Brown A, Collier C, Pineda M-C, Robson B, Uthicke S, Waterhouse J (2025) The seven sins of climate change: a review of rates of change, and quantitative impacts on ecosystems and water quality in the Great Barrier Reef. *Marine Pollution Bulletin* **219**, 118267. doi:10.1016/j.marpolbul.2025.118267

Friess DA, Rogers K, Lovelock CE, Krauss KW, Hamilton SE, Lee SY, Lucas R, Primavera J, Rajkaran A, Shi S (2019) The state of the world's mangrove forests: past, present, and future. *Annual Review of Environment and Resources* **44**(1), 89–115. doi:10.1146/annurev-environ-101718-033302

Friis K, Körtzinger A, Wallace DWR (2003) The salinity normalization of marine inorganic carbon chemistry data. *Geophysical Research Letters* **30**(2), 1085. doi:10.1029/2002GL015898

George LW, Martins APB, Heupel MR, Simpfendorfer CA (2019) Fine-scale movements of juvenile blacktip reef sharks *Carcharhinus melanopterus* in a shallow nearshore nursery. *Marine Ecology Progress Series* **623**, 85–97. doi:10.3354/meps13010

Gordon SE, Goatley CHR, Bellwood DR (2016) Composition and temporal stability of turf sediments on inner-shelf coral reefs. *Marine Pollution Bulletin* **111**(1–2), 178–183. doi:10.1016/j.marpolbul.2016.07.013

Harianto J, Aldridge J, Torres Gabarda SA, Grainger RJ, Byrne M (2021) Impacts of acclimation in warm–low pH conditions on the physiology of the sea urchin *Heliocidaris erythrogramma* and carryover effects for juvenile offspring. *Frontiers in Marine Science* **7**, 588938. doi:10.3389/fmars.2020.588938

Harper KA, Macdonald SE, Burton PJ, Chen J, Brosofske KD, Saunders SC, Euskirchen ES, Roberts D, Jaiteh MS, Esseen P-A (2005) Edge influence on forest structure and composition in fragmented landscapes. *Conservation Biology* **19**(3), 768–782. doi:10.1111/j.1523-1739.2005.00045.x

Hopley D, Smithers SG, Parnell K (2007) 'The geomorphology of the Great Barrier Reef: development, diversity and change.' (Cambridge University Press) doi:10.1017/CBO9780511535543

Jankowski JE, Kyle KO, Gasner MR, Ciecka AL, Rabenold KN (2021) Response of avian communities to edges of tropical montane forests: implications for the future of endemic habitat specialists. *Global Ecology and Conservation* **30**, e01776. doi:10.1016/j.gecco.2021.e01776

Jeffrey SW, Humphrey GF (1975) New spectrophotometric equations for determining chlorophylls a, b, c and c_2 in higher plants, algae and natural phytoplankton. *Biochemie und Physiologie der Pflanzen* **167**(2), 191–194. doi:10.1016/S0015-3796(17)30778-3

Karimpour A, Chen Q (2017) Wind wave analysis in depth limited water using *OCEANLYZ*, a *MATLAB* toolbox. *Computers & Geosciences* **106**, 181–189. doi:10.1016/j.cageo.2017.06.010

Kleypas JA, Anthony KRN, Gattuso J-P (2011) Coral reefs modify their seawater carbon chemistry – case study from a barrier reef (Moorea, French Polynesia). *Global Change Biology* **17**(12), 3667–3678. doi:10.1111/j.1365-2486.2011.02530.x

Krauss KW, Ball MC (2013) On the halophytic nature of mangroves. *Trees* **27**(1), 7–11. doi:10.1007/s00468-012-0767-7

Laurance WF, Yensen E (1991) Predicting the impacts of edge effects in fragmented habitats. *Biological Conservation* **55**(1), 77–92. doi:10.1016/0006-3207(91)90006-U

Li J, Heap AD (2008) 'A review of spatial interpolation methods for environmental scientists.' (Geoscience Australia: Canberra, ACT, Australia)

Lugo AE, Snedaker SC (1974) The ecology of mangroves. *Annual Review of Ecology and Systematics* **5**, 39–64. doi:10.1146/annurev.es.05.110174.000351

Maggioni F, Pujo-Pay M, Aucan J, Cerrano C, Calcinai B, Payri C, Benzoni F, Letourneur Y, Rodolfo-Metalpa R (2021) The Bouraké semi-enclosed lagoon (New Caledonia) – a natural laboratory to study the lifelong adaptation of a coral reef ecosystem to extreme environmental conditions. *Biogeosciences* **18**(18), 5117–5140. doi:10.5194/bg-18-5117-2021

Mehrbach C, Culberson CH, Hawley JE, Pytkowicx RM (1973) Measurement of the apparent dissociation constants of carbonic acid in seawater at atmospheric pressure. *Limnology and Oceanography* **18**(6), 897–907. doi:10.4319/lo.1973.18.6.0897

Mos B, Holloway C, Kelaher BP, Santos IR, Dworjanyn SA (2021) Alkalinity of diverse water samples can be altered by mercury preservation and borosilicate vial storage. *Scientific Reports* **11**, 9961. doi:10.1038/s41598-021-89110-w

Murcia C (1995) Edge effects in fragmented forests: implications for conservation. *Trends in Ecology & Evolution* **10**(2), 58–62. doi:10.1016/S0169-5347(00)88977-6

Oakley-Cogan A, Tebbett SB, Bellwood DR (2020) Habitat zonation on coral reefs: structural complexity, nutritional resources and herbivorous fish distributions. *PLoS ONE* **15**(6), e0233498. doi:10.1371/journal.pone.0233498

O'Keeffe MJ (1991) Over and under: geography and archaeology of the Palm Islands. PhD thesis. James Cook University of North Queensland, Townsville, QLD, Australia. doi:10.25903/5bd64ed3b88c4

Page HN, Andersson AJ, Jokiel PL, Rodgers KS, Lebrato M, Yeakel K, Davidson C, D'Angelo S, Bahr KD (2016) Differential modification of seawater carbonate chemistry by major coral reef benthic communities. *Coral Reefs* **35**(4), 1311–1325. doi:10.1007/s00338-016-1490-4

Page HN, Courtney TA, De Carlo EH, Howins NM, Koester I, Andersson AJ (2019) Spatiotemporal variability in seawater carbon chemistry for a coral reef flat in Kāne'ohe Bay, Hawai'i. *Limnology and Oceanography* **64**(3), 913–934. doi:10.1002/lno.11084

Pedersen K, Cyronak T, Goodrich M, Kline DI, Linsmayer LB, Torres R, Tresguerres M, Andersson AJ (2024) Short-term spatiotemporal variability in seawater carbonate chemistry at two contrasting reef locations in Bocas del Toro, Panama. *Aquatic Geochemistry* **30**(1), 1–29. doi:10.1007/s10498-024-09421-y

Pezner AK, Courtney TA, Barkley HC, Chou W-C, Chu H-C, Clements SM, Cyronak T, DeGrandpre MD, Kekuewa SAH, Kline DI, *et al.* (2023) Increasing hypoxia on global coral reefs under ocean warming. *Nature Climate Change* **13**(4), 403–409. doi:10.1038/s41558-023-01619-2

Reithmaier GMS, Ho DT, Johnston SG, Maher DT (2020) Mangroves as a source of greenhouse gases to the atmosphere and alkalinity and dissolved carbon to the coastal ocean: a case study from the Everglades National Park, Florida. *Journal of Geophysical Research: Biogeosciences* **125**(12), e2020JG005812. doi:10.1029/2020JG005812

Reithmaier GMS, Cabral A, Akhand A, Bogard MJ, Borges AV, Bouillon S, Burdige DJ, Call M, Chen N, Chen X, *et al.* (2023) Carbonate chemistry and carbon sequestration driven by inorganic carbon outwelling from mangroves and saltmarshes. *Nature Communications* **14**, 8196. doi:10.1038/s41467-023-44037-w

Ries L, Sisk TD (2004) A predictive model of edge effects. *Ecology* **85**(11), 2917–2926. doi:10.1890/03-8021

Saderne V, Baldry K, Anton A, Agustí S, Duarte CM (2019) Characterization of the CO_2 system in a coral reef, a seagrass meadow, and a mangrove

Downloaded from connectsci.au/mf/article-pdf/doi/10.1071/MF25151/1972128/mf25151.pdf by guest on 25 November 2026

forest in the central Red Sea. *Journal of Geophysical Research: Oceans* **124**(11), 7513–7528. doi:10.1029/2019JC015266

Saderne V, Fusi M, Thomson T, Dunne A, Mahmud F, Roth F, Carvalho S, Duarte CM (2021) Total alkalinity production in a mangrove ecosystem reveals an overlooked Blue Carbon component. *Limnology and Oceanography Letters* **6**(2), 61–67. doi:10.1002/lol2.10170

Scucchia F, Zaslansky P, Boote C, Doheny A, Mass T, Camp EF (2023) The role and risks of selective adaptation in extreme coral habitats. *Nature Communications* **14**, 4475. doi:10.1038/s41467-023-39651-7

Shaw EC, McNeil BI, Tilbrook B (2012) Impacts of ocean acidification in naturally variable coral reef flat ecosystems. *Journal of Geophysical Research: Oceans* **117**(C3), C03038. doi:10.1029/2011JC007655

Sippo JZ, Maher DT, Tait DR, Holloway C, Santos IR (2016) Are mangroves drivers or buffers of coastal acidification? Insights from alkalinity and dissolved inorganic carbon export estimates across a latitudinal transect. *Global Biogeochemical Cycles* **30**(5), 753–766. doi:10.1002/2015GB005324

Stewart HA, Kline DI, Chapman LJ, Altieri AH (2021) Caribbean mangrove forests act as coral refugia by reducing light stress and increasing coral richness. *Ecosphere* **12**(3), e03413. doi:10.1002/ecs2.3413

Stewart HA, Wright JL, Carrigan M, Altieri AH, Kline DI, Araújo RJ (2022) Novel coexisting mangrove–coral habitats: extensive coral communities located deep within mangrove canopies of Panama, a global classification system and predicted distributions. *PLoS ONE* **17**(6), e0269181. doi:10.1371/journal.pone.0269181

Suzuki A, Kawahata H (2003) Carbon budget of coral reef systems: an overview of observations in fringing reefs, barrier reefs and atolls in the Indo-Pacific regions. *Tellus B – Chemical and Physical Meteorology* **55**(2), 428–444. doi:10.3402/tellusb.v55i2.16761

Takeshita Y, Cyronak T, Martz TR, Kindeberg T, Andersson AJ (2018) Coral reef carbonate chemistry variability at different functional scales. *Frontiers in Marine Science* **5**, 175. doi:10.3389/fmars.2018.00175

Tanner JE (2005) Edge effects on fauna in fragmented seagrass meadows. *Austral Ecology* **30**(2), 210–218. doi:10.1111/j.1442-9993.2005.01438.x

Volta C, Ho DT, Maher DT, Wanninkhof R, Friederich G, Del Castillo C, Dulai H (2020) Seasonal variations in dissolved carbon inventory and fluxes in a mangrove-dominated estuary. *Global Biogeochemical Cycles* **34**(12), e2019GB006515. doi:10.1029/2019GB006515

Waller A, Byrne M, Foo SA (2025) Coexisting mangrove-coral habitats: trends in seawater chemistry and implications for corals. In 'Oceanography and marine biology. Vol. 63'. (Eds BD Russell, PA Todd) pp. 97–113. (CRC Press) doi:10.1201/9781003589600-3

Wolfe K, Vidal-Ramirez F, Dove S, Deaker D, Byrne M (2018) Altered sediment biota and lagoon habitat carbonate dynamics due to sea cucumber bioturbation in a high-pCO_2 environment. *Global Change Biology* **24**(1), 465–480. doi:10.1111/gcb.13826

Wolfe K, Nguyen HD, Davey M, Byrne M (2020) Characterizing biogeochemical fluctuations in a world of extremes: a synthesis for temperate intertidal habitats in the face of global change. *Global Change Biology* **26**(7), 3858–3879. doi:10.1111/gcb.15103

Wolfe K, Deaker DJ, Graba-Landry A, Champion C, Dove S, Lee R, Byrne M (2021) Current and future trophic interactions in tropical shallow-reef lagoon habitats. *Coral Reefs* **40**(1), 83–96. doi:10.1007/s00338-020-02017-2

Yates KK, Rogers CS, Herlan JJ, Brooks GR, Smiley NA, Larson RA (2014) Diverse coral communities in mangrove habitats suggest a novel refuge from climate change. *Biogeosciences* **11**(16), 4321–4337. doi:10.5194/bg-11-4321-2014

Zuur AF, Ieno EN, Elphick CS (2010) A protocol for data exploration to avoid common statistical problems. *Methods in Ecology and Evolution* **1**(1), 3–14. doi:10.1111/j.2041-210X.2009.00001.x

Ethics approval. Ethics approval is not applicable for this research.

Data availability. The data that support this study are avilable within the article and its supplementary material.

Conflicts of interest. The authors declare that they have no conflicts of interest.

Declaration of funding. This work was supported by the Australian Research Council (Grant numbers: DE220100555 to S. A. Foo, DP220101125 to M. Byrne); the Westpac Scholars Trust (Westpac Research Fellowship to S. A. Foo); the University of Sydney (Horizon Fellowship to S. A. Foo); and the Orpheus Island Research Station Morris Family Trust (Student Research Grant to A. Waller).

Acknowledgements. We thank the staff at Orpheus Island Research Station for their support in facilitating and conducting fieldwork, and Sergio Torres at the Sydney Institute of Marine Science for his assistance with total alkalinity analysis. We also gratefully acknowledge HydroTerra and PyroScience for lending us the AquapHOx-L-O2 and AquapHOx-L-pH loggers for the duration of this project, and for their helpful advice in correcting measured values.

Author contributions. A. Waller led the study and, together with S. Foo and M. Byrne, developed the research question and study design. A. Waller and S. Foo acquired funding for the project. A. Waller, M. Webb and S. Foo conducted the field sampling. L. Perris assisted with wave-data analysis, and T. White contributed to the statistical analysis. K. Wolfe supported manuscript preparation and editing. A. Waller, K. Wolfe and S. Foo wrote the paper, with editing from M. Byrne. All authors approved the final submission.

Author affiliations

[A]Marine Invertebrate Futures Group, School of Life and Environmental Sciences, The University of Sydney, Sydney, NSW 2006, Australia.

[B]Marine Biology and Ecology Consultant, Geeveston, TAS 7116, Australia.

[C]Geocoastal Research Group and Marine Studies Institute, School of Geosciences, The University of Sydney, Sydney, NSW 2006, Australia.

Downloaded from connectsci.au/mf/article-pdf/doi/10.1071/MF25151/1972128/mf25151.pdf by guest on 25 November 2026